Spatial heterogeneity in aeolian erodibility: Uniform, topographic, geomorphic, and hydrologic hypotheses

Charles S. Zender and David Newman
Department of Earth System Science, University of California at Irvine, Irvine, California, USA

Omar Torres
Joint Center for Earth Systems Technology, University of Maryland Baltimore County, Baltimore, Maryland, USA

Received 12 October 2002; revised 26 February 2003; accepted 31 March 2003; published 9 September 2003.

[1] Soil aeolian erodibility is the efficiency with which soil produces dust for a given meteorological forcing. Quantifying soil erodibility is crucial for forecasting dust events and the climatological distribution and forcing of dust. We use long-term station observations and satellite indices of mineral dust to ascertain the role of regional topography, geomorphology, and hydrology in controlling sediment availability and erodibility. Our null hypothesis is that soil erodibility is globally uniform, so that emissions are determined by instantaneous local meteorology, vegetation, and soil moisture. We describe and quantify three competing hypotheses on regional processes which may affect local soil erodibility: (1) Erodibility is characterized by the relative elevation of source regions in surrounding basins. (2) Erodibility is characterized by the upstream area from which sediments may have accumulated locally through all climate regimes. (3) Erodibility is characterized by the local present-day surface runoff. These hypotheses are tested in 3-year simulations of the global Dust Entrainment and Deposition (DEAD) model. All three spatially varying erodibility hypotheses produce significantly better agreement with station and satellite data than the null (Uniform) hypothesis. The Uniform hypothesis explains none of the spatial structure of emissions in Australia. Heterogeneous erodibility may explain up to 15–20%, 15–20%, and 50% more of the spatial structure of dust emissions than Uniform erodibility in the Sahara+Arabian Peninsula, East Asia, and Australia, respectively. The Geomorphic erodibility hypothesis performs best overall, but results vary by region and by metric. These results support the hypothesis that dust emission ''hot spots'' exist in regions where alluvial sediments have accumulated and may be disturbed. Our physically based erodibility hypotheses help explain dust observations in some regions, particularly East Asia, and can be used to help discriminate between natural and anthropogenic soil emissions. *INDEX TERMS:* 0305 Atmospheric Composition and Structure: Aerosols and particles (0345, 4801); 1625 Global Change: Geomorphology and weathering (1824, 1886); 1815 Hydrology: Erosion and sedimentation; 1824 Hydrology: Geomorphology (1625); *KEYWORDS:* mineral dust aerosol, arid geomorphology, aeolian processes, hydrologic routing, landscape erodibility

Citation: Zender, C. S., D. Newman, and O. Torres, Spatial heterogeneity in aeolian erodibility: Uniform, topographic, geomorphic, and hydrologic hypotheses, *J. Geophys. Res.*, *108*(D17), 4543, doi:10.1029/2002JD003039, 2003.

1. Introduction

[2] Mineral dust aerosol plays important chemical, radiative, and biogeochemical roles in the Earth system. Explaining the observed spatial heterogeneity of global dust emissions is important for understanding the relative role of natural and anthropogenic processes in the present-day dust emissions, and thus for predicting future trends in dust production [*Penner et al.*, 2001]. The global distribution of mineral dust is difficult to predict because of the strong sensitivity of dust emission to poorly known boundary conditions such as soil texture, cohesiveness, and boundary layer conditions [e.g., *Gillette*, 1978; *Schulz et al.*, 1996]. We identify related topographic, geomorphic, and hydrologic processes which may constrain this heterogeneity. Using the global Dust Entrainment and Deposition (DEAD) model [*Zender et al.*, 2003], we investigate the effect of each process relative to a control simulation with no imposed spatial heterogeneity. We show that, in almost all cases, the incorporation of regional topographic, geomorphic, and hydrologic influences improves the dust simulations.

[3] Satellite observations show that persistent maxima in the observed mineral aerosol distribution are associated with underlying topographic basins [*Prospero et al.*, 2002]. These maxima have been termed ''hot spots'' [*Gillette*,

0148-0227/03/2002JD003039$09.00

1999] and one hypothesis for their formation, advanced by Prospero et al., is that loose alluvial sediments, which are highly erodible, preferentially accumulate in these basins. The apparent enhanced erodibility of sediments in these basins may be due to their high concentration of clay and silt-sized particles, or to intermittent disturbance of these soils by hydrologic or other processes.

[4] These sediments may be responsible for greater dust emission efficiencies (i.e., erodibility) than comparable locations which lack hydrologically disturbed/renewed sediments. Dust models which attempt to account for sediment-rich source regions succeed in reproducing significant spatial features of the dust distribution [*Ginoux et al.*, 2001; *Zender et al.*, 2003; C. Luo et al., A 22-year climatology of mineral aerosols, submitted to *Journal of Geophysical Research*, 2003] (hereinafter referred to as Luo et al., submitted manuscript, 2003). However, the extent to which parameterizations of erodibility are required to explain the observed dust record, and the physical basis of such parameterizations, remain unknown. Dust from anthropogenic disturbances complicates the observed record since it is very difficult to distinguish from natural dust, whether far downwind or near to topographic basins [*Mahowald et al.*, 2002].

[5] Dust emissions are directly related to wind speed, atmospheric stability, surface roughness, vegetative cover, gross soil texture, and soil moisture [e.g., *Marticorena and Bergametti*, 1995]. In addition, emissions show large variations attributable to other soil characteristics such as parent soil (saltator) texture, fine particle aggregation, soil modulus of rupture, and degree of disturbance. The second group of properties are related to current and past hydrologic activity because precipitation and surface runoff in and upstream of dust sources are linked to local soil abundance, size, chemical properties, and disturbance history.

[6] Regions with erodibility higher than can be accounted for by instantaneous meteorological conditions appear as biases in dust production models. We define the dust source erodibility S as the ratio of actual vertical dust mass flux F_d to the mass flux $F_{d,0}$ mobilized from an idealized surface in the absence of regional geographic influences. Thus S is intended to represent the influence of regional topography, geomorphology, and hydrology on dust emissions. If regional geomorphic and hydrologic processes are unimportant in explaining present-day dust emissions, then global simulations using a constant factor $S = S_0$ should perform no worse than simulations which account for regional heterogeneity, i.e., $S = S(x, y)$ where x and y represent latitude and longitude, respectively.

[7] The paper is organized as follows. Section 2 describes the dust model, erodibility hypotheses, and observational data sets. Section 3 presents results of the erodibility hypotheses in global simulations and statistical intercomparisons to three observed data sets. Section 4 summarizes our findings and recommendations for future research on the Aeolian erodibility of global soils.

2. Methods

2.1. Model Description

[8] We examine the global atmospheric mineral dust distribution and its sensitivity to topographic, geomorphic, and hydrologic constraints on source sediment availability in the Dust Entrainment and Deposition (DEAD) model. The DEAD model and these erodibility factors are available to all interested researchers. Visit the model homepage (http://dust.ess.uci.edu/dead) or contact the authors for details. The interested reader is referred to *Zender et al.* [2003] for the full model description and evaluation of a 10-year (1990–1999) model dust climatology.

[9] The salient physical processes represented in DEAD are as follows: DEAD determines the kinematic and thermodynamic properties of the boundary layer by assuming that the surface and atmosphere constantly adjust surface heat, vapor, and momentum exchanges to maintain thermal equilibrium with the radiation field [*Bonan*, 1996]. We account for these adjustments when computing the drag generated by surface winds blowing over bare ground and vegetation. This solution of the boundary layer turbulence problem determines the modeled wind friction speed. The dust model idealizes dust entrainment due to saltation of the parent soil population [*White*, 1979]. When the wind friction speed exceeds the threshold friction speed [*Iversen and White*, 1982], ballistic impacts cause disaggregated sand, silt, and clay-sized particles to become entrained [*Marticorena and Bergametti*, 1995] in proportion to observed size distributions [*D'Almeida*, 1987; *Schulz et al.*, 1998]. We also impose additional constraints on saltation and entrainment due to surface soil moisture, vegetation, and drag partition [*Gillette et al.*, 1998; *Fécan et al.*, 1999].

[10] The inputs to DEAD are boundary layer wind speeds, soil texture and hydrology, leaf and stem area index, solar and thermal radiative fluxes (to determine stability), and local topography. Given these inputs, the model predicts the horizontal saltation mass flux Q_s and the size-resolved vertical dust entrainment flux $F_{d,j}$ using equation (17) of *Zender et al.* [2003]:

$$F_{d,j} = TA_m S \alpha Q_s \sum_{i=1}^{I} M_{i,j} \tag{1}$$

where T is a globally uniform tuning factor, A_m is the fraction of bare soil exposed in a gridcell, α is the saltation-sandblasting mass efficiency [*Alfaro et al.*, 1997], and $M_{i,j}$ is the mass fraction of each source mode i carried in each transport bin j. Equation (1) shows that the vertical mass flux of dust $F_{d,j}$ varies linearly with S. In this study, S is the only factor in equation (1) that is allowed to vary among the experiments.

[11] The entrained mass $F_{d,j}$ (equation (1)) is transported, and then ultimately removed from the atmosphere by dry and wet deposition removal processes as formulated by *Seinfeld and Pandis* [1997]. The instantaneous atmospheric mass concentration of dust is the residual of these source and sink processes.

2.2. Satellite Observations

[12] We use three independent data sets to evaluate the verisimilitude of each erodibility hypothesis. These data sets contain surface observations of dust mass concentration, surface observations of dust mass deposition, and satellite indices of aerosol absorption. This combination allows us to make quantitative evaluations at select locations which sample dusty and dust-free regions globally, with more

qualitative evaluations of the overall dust distribution in source regions.

[13] Improvements in the erodibility factor S should be most apparent in dust source regions, before transport and diffusion disguise the spatial origin of the dust. The longest global data set of dust distribution over land is presently derived from the Total Ozone Mapping Spectrometer (TOMS) instrument. TOMS instruments have been continually measuring reflected UV radiances at multiple wavelengths since 1980 (except between May 1993 and July 1996). *Herman et al.* [1997] and *Torres et al.* [1998] describe the construction of the TOMS Absorbing Aerosol Index (AAI) from these radiances. The relation between AAI and the optical depth of absorbing aerosol is spatially dependent but generally linear [*Chiapello et al.*, 1999; *Hsu et al.*, 1999]. As such, AAI is a useful proxy for the spatial distribution of absorbing aerosol [*Prospero et al.*, 2002].

[14] The robustness of conclusions reached from intercomparing AAI with models is limited. First, the AAI for a given mass of aerosol varies approximately linearly with the aerosol height [*Hsu et al.*, 1999] and is insensitive to absorbing aerosol in the lowest 1 km [*Torres et al.*, 1998]. N. M. Mahowald et al. (Sensitivity of the TOMS aerosol index to boundary layer height: Implications for detection of mineral aerosol sources, submitted to *Geophysical Research Letters*, 2003) (hereinafter referred to as Mahowald et al., submitted manuscript, 2003) show how regional variations in boundary layer height may bias AAI as a measure of total column absorbing aerosol. Second, the AAI does not discriminate between absorbing carbonaceous aerosols and mineral aerosols. Third, the AAI uses a minimum threshold for detection so it is relatively insensitive to small amounts of aerosol. *Torres et al.* [2002] recently constructed a long-term record of Aerosol Optical Depth (AOD) at 380 nm from TOMS data. This TOMS AOD removes some limitations of the AAI by estimating the species, composition, size, and height of the aerosol layer.

[15] Our strategy to improve model comparison with TOMS is twofold. First, we reduce contamination from biomass burning aerosol by focusing on desert regions. We eliminate points with significant vegetation, defined as a mean seasonally varying vegetation leaf + stem area index $V > 0.3$ m^2 m^{-2} [*Kergoat et al.*, 1999; *Zender et al.*, 2003]. Second, we compare against both the TOMS AAI and AOD. Our results focus on TOMS AAI because it excludes nonabsorbing aerosols, but we also use TOMS AOD where it provides additional insight. We use all available TOMS data from 1980–2001 because we seek to improve understanding of dust source regions in the present climate, not just the simulation time period (1990–1992). However, our results do not change qualitatively when we compare to 1990–1992 alone, nor when we exclude post-1993 (when TOMS changed sensors) data.

2.3. Surface Observations

[16] Next we intercompared surface mass concentrations of each simulation with observations at sites managed by the Rosenstiel School of Marine and Atmospheric Science (RSMAS) at the University of Miami. Station locations [*Ginoux et al.*, 2001; *Woodward*, 2001] and sampling techniques [*Savoie et al.*, 1992; *Maring et al.*, 2000] are discussed in the literature. These measurements were made by ashing air filters and weighing the remaining nonvolatile aerosol mass, or by estimating dust mass from neutron activation analysis of aluminum abundance (assuming dust is 8% aluminum by mass). As a result, the University of Miami dust data set is unlikely to be contaminated by other aerosol species. We present comparisons against climatological monthly and annual mean concentrations from stations with between one-half year (Cape Point) to 18 years (Barbados) of data, weighting the observations equally regardless of the record length.

[17] Finally we intercompared long-term land-based measurements of surface deposition fluxes. Unlike marine sediments, land deposition fluxes reflect only atmospheric transport. Our comparisons are against 11 locations compiled by *Ginoux et al.* [2001]. These stations span both hemispheres and approximately 90-station-years of measurements from the 1950s to the present. The majority of the stations were most active in the 1980s, and lay outside of our simulation period. The 10-year (1990–1999) DEAD dust climatology shows reasonable agreement with the TOMS, University of Miami concentration, and deposition observations [*Zender et al.*, 2003].

2.4. Uniform Erodibility

[18] We performed four 3-year global dust simulations, a control and three experiments. In the control simulation, called "Uniform," regional geographic properties are neglected so that $S = S_0 = 5.707$ globally. This S is used in equation (1) but for clarity in intercomparing erodibility factors we present each S normalized by 5.707 so that a value of $S = 1.0$ at any point is equivalent to Uniform erodibility. Figure 1 shows the source erodibility S/S_0 determined by each erodibility hypothesis. S spans more than 2 orders of magnitude. The contrast between the uniform and the heterogeneous S is striking.

2.5. Topographic Erodibility

[19] The Topographic hypothesis, called "Topo," tests the influence of topographic basins using the basin factor of *Ginoux et al.* [2001]. Ginoux et al. parameterized S_i, the erodibility factor at gridcell i, as

$$S_i = \left(\frac{z_{\max} - z_i}{z_{\max} - z_{\min}} \right)^5 \tag{2}$$

where z_i is the local mean surface elevation, and $z_{\max}$ and $z_{\min}$ are the maximum and minimum elevations in the surrounding $10^\circ \times 10^\circ$ region. This region size was determined through trial and error. The exponent of 5 in equation (2) was chosen to produce approximate agreement between predictions and observations such as the TOMS AAI. The topographic source factor (2) is quasi-local in nature: S_i does not depend on the properties of neighboring gridcells, only on $z_{\max}$ and $z_{\min}$.

2.6. Geomorphic Erodibility

[20] The Geomorphic hypothesis, dubbed "Geo," defines S proportional to the upstream runoff collection area, i.e., the upstream area from which surface runoff may reach a given location. This area depends on the regional topography but does not depend on actual runoff, so we call it the geomorphic basin area. Here S_i represents the sum of the

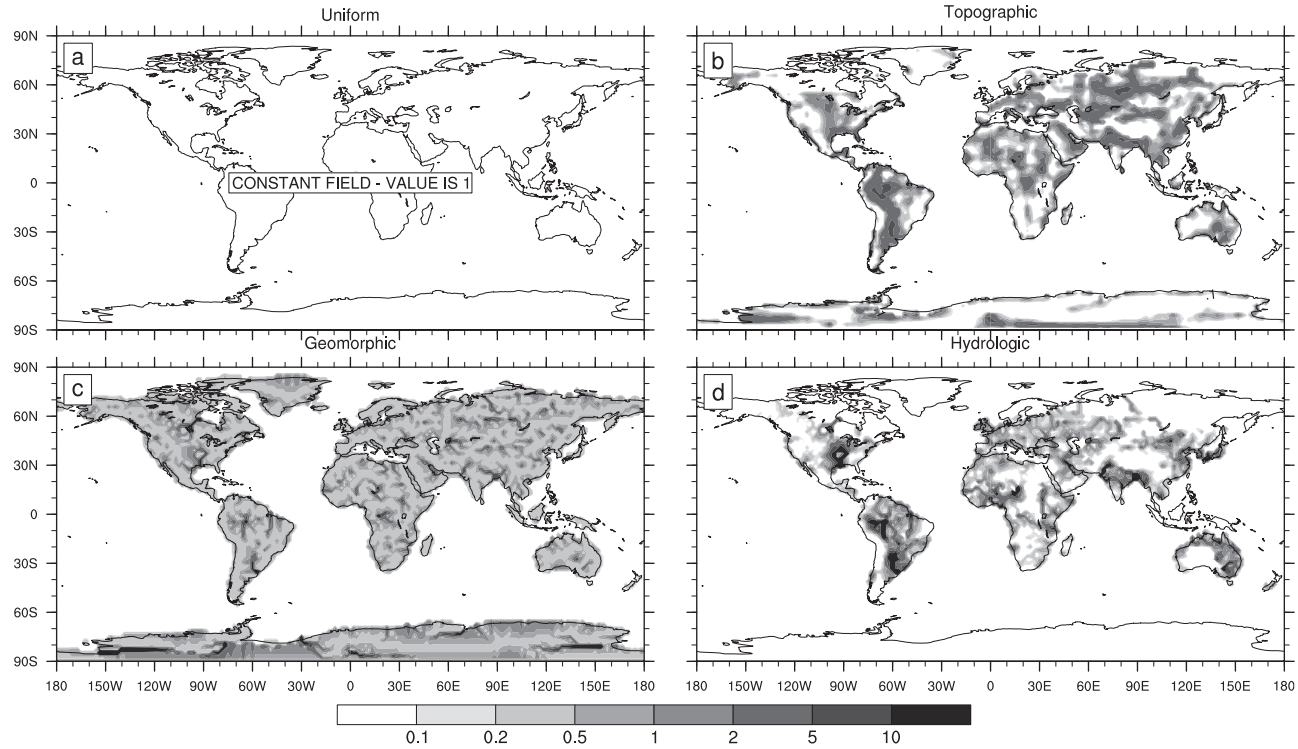

Figure 1. Soil erodibility S for four hypotheses: (a) Uniform, (b) Topographic, (c) Geomorphic, and (d) Hydrologic.

area of all gridcells that flow into gridcell i, normalized by the global maximum flow into any cell, $\max(S_i)$. We compute S_i using the two step procedure described by *Jenson and Domingue* [1988]. First the flow direction at each gridcell i is determined, then the area of gridcells upstream of i is summed. The flow direction at each gridcell i is chosen to be toward the lowest (in elevation) of the eight neighboring gridcells that surround gridcell i. In most cases, there is a unique lowest neighbor, so this choice is straightforward. Other cases require further treatment (ties between two equally low neighbors are resolved randomly) and planar situations (two or more lowest neighbors that are at same elevation as point i) are resolved iteratively. Summing the area of upstream gridcells is analogous to counting leaves on a tree beyond any point on a branch: first we sort the gridcells from highest elevation to lowest elevation, then starting with the highest cell, we accumulate the area of the flow into gridcell i. Planar situations need to be set recursively, accumulating upstream gridcells first. We applied this procedure to a Digital Elevation Map (NGDC 5-minute TerrainBase DEM) regridded to the T62 horizontal resolution ($\sim 1.9^\circ \times 1.9^\circ$) of the dust transport model [*Zender et al.*, 2003]. We verified the basin areas by checking that, for any given region, the sum of S_i at all points on the area's perimeter plus S_i at all internal basins was equal to the area of the region.

[21] The algorithm outlined above produces unrealistic internal drainages in some important hydrologic basins. The algorithm identifies multiple cell internal basins as local drainage sinks and does not propogate their drainage area to the coast. This is correct in many important dust source regions that are internally drained, such as the Bodele Depression, the Tarim Basin, the Aral Sea region, and the Lake Eyre basin. However the algorithm incorrectly identifies some ocean drainage basins, such as the Amazon basin, as internal. In reality these basins drain into the next basin or ocean through so-called pour points which contain unresolved drainage features (e.g., channels). In this work we have not forced false internal basins to drain to the sea and mimic present-day river courses. The result is that the Geomorphic and Hydrologic erodibility factors S are based on smaller than actual drainage basins in some regions. This has a negligible effect on dust production in basins that are currently very wet (like the Amazon), since vegetation and soil moisture inhibit soil deflation anyway. The bias is greatest in basins with arid downstream regions, such as the Nile. We plan to reduce this bias in the future by using more sophisticated drainage algorithms.

2.7. Hydrologic Erodibility

[22] The Hydrologic hypothesis, dubbed ''Hydro,'' defines S proportional to the surface hydrologic flow through each point. The overland hydrologic flow through each gridcell is the sum of the local runoff with the runoff from each upstream neighbor. It is at first counterintuitive that dust sources should preferentially be located in active drainage basins. However, field evidence suggests that arid regions which are sediment-limited may become more active dust sources after temporary hydrologic activity or inundation replenishes the sediment supply. This behavior has been observed on clay pans in the northern Lake Eyre Basin in Australia [*McTainsh et al.*, 1999]. Too much hydrologic activity quenches dust production because consistently high soil moisture results in standing vegetation.

[23] Here surface runoff was obtained from a 20-year present-day simulation of the NCAR Land Surface Model

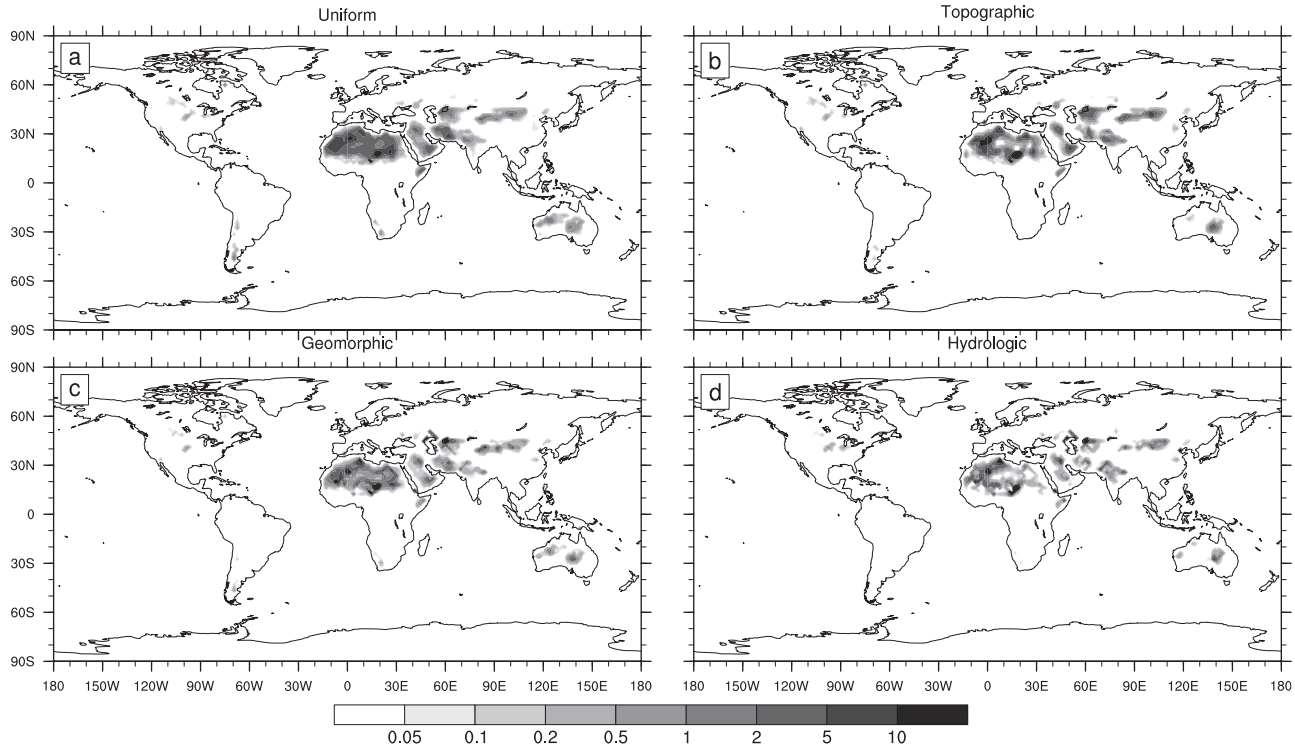

Figure 2. Predicted annual mean mass emissions flux [$\mu g\ m^{-2}\ s^{-1}$] for (a) Uniform *S*, (b) Topographic *S*, (c) Geomorphic *S*, and (d) Hydrologic *S*. Scale is logarithmic.

(LSM) [*Bonan et al.*, 2002]. The LSM uses hand-corrected flow directions [*Graham et al.*, 1999] so runoff predictions do not suffer from unrealistic internal drainage basins. We note that basing erodibility on present-day hydrology does not test the alternate hypothesis that present-day erodibility is controlled by sediments accumulated in past climates when runoff differed. Indeed, our future work will include testing the hypothesis that present-day emissions from Africa are from deposits accumulated during the moister Saharan climate of the mid-Holocene.

3. Results

[24] We evaluate the consequences and efficacy of each erodibility hypothesis (uniform, topographic, geomorphic, hydrologic) in the DEAD model [*Zender et al.*, 2003] forced by interpolated 6-hourly NCEP winds [*Kalnay*, 1996] on a T62L28 grid for the years 1990–1992. The 1990–1992 model climatology is similar to the climatological behavior of the model over the period encompassing all the observations (1980–2001) [*Zender et al.*, 2003; Luo et al., submitted manuscript, 2003; *Mahowald et al.*, 2003]. The four 3-year simulations were tuned a posteriori to produce identical annual mean atmospheric mass burdens of dust. Thus differences in the statistics of the dust distribution are due to the spatial distribution of sources, and to regional differences in the efficiency of sink processes, especially wet deposition.

3.1. Mobilization, Burden, and Deposition

[25] Figure 2 shows the climatological (1990–1992) mean emitted mass flux [$\mu g\ m^{-2}\ s^{-1}$] for each erodibility hypothesis. Given the great disparity in *S* among the cases (Figure 1), the similarity in emissions flux is surprising. In all four cases emissions are predominantly from the global dust belt, as is observed [*Prospero et al.*, 2002]. This consistency demonstrates the importance of vegetation, surface wetness, and meteorological constraints on aeolian erosion, as these factors are not considered in *S*.

[26] Uniform erodibility (Figure 2a) results in the least structured emissions, with more diffuse source regions than the other cases, especially in North Africa. The Topographic and Geomorphic cases both show more structure in the Libyan desert region, with distinct features near the Mourdi Depression and northwestern Egypt. These structured features are also seen in TOMS AAI imagery (see Figure 5 below). The Hydrologic hypothesis causes the most concentrated source regions. This is expected because the structure imposed by accumulated upstream area is enhanced by the structure of active present-day surface runoff.

[27] The Uniform, Geomorphic and Hydrologic experiments capture the source at the Etosha Pan in Northern Namibia [*Prospero et al.*, 2002], but also contain an apparently fictitious source near 30S, 20E in South Africa. All hypotheses show unrealistically strong sources in the Great Plains in North America and Southern Canada. Dust from these relatively weak sources in the Americas washes out quickly and does not travel far.

[28] On the basis of emission fluxes alone, none of the competing hypotheses can be excluded as unrealistic because climatological measurements of emissions in the global dust belt are virtually nonexistent. Satellite sensors and passive surface samplers observe dust in the atmosphere or deposited at the surface, so we next examine those quantities.

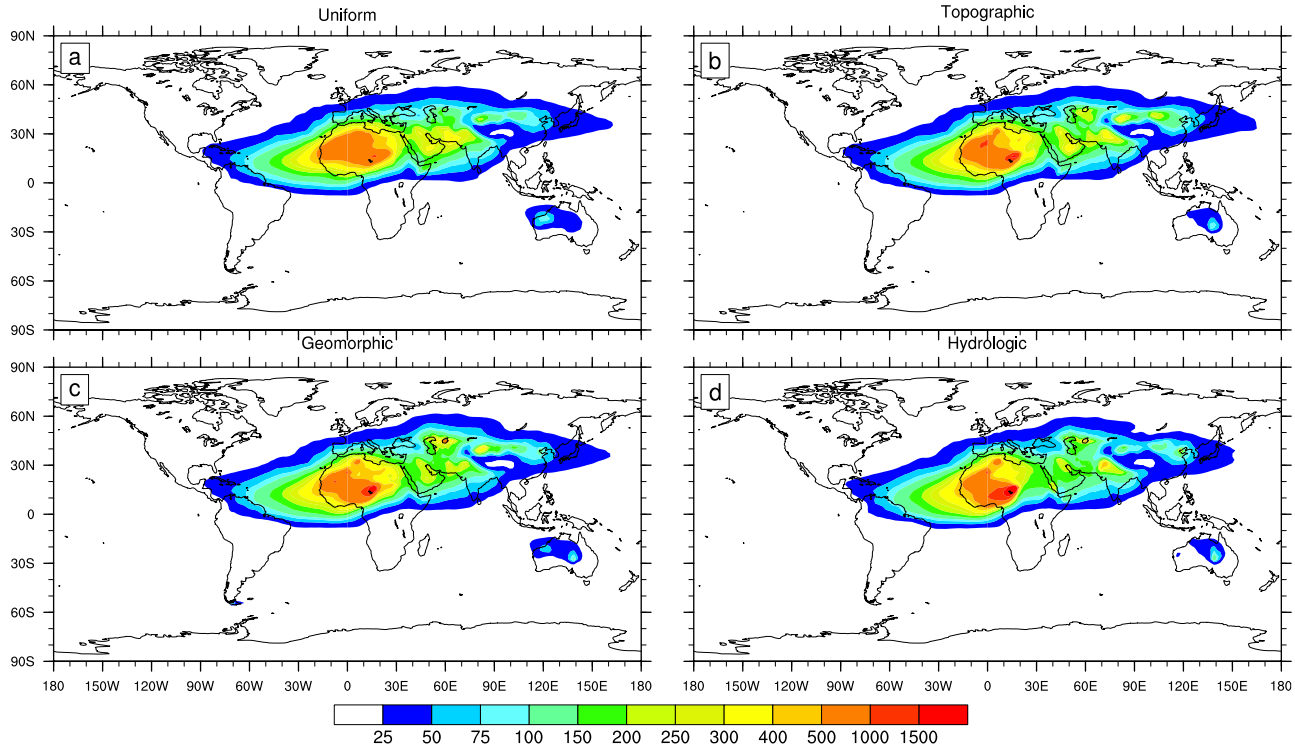

Figure 3. Predicted annual mean dust burden [mg m^{-2}] for (a) Uniform *S*, (b) Topographic *S*, (c) Geomorphic *S*, and (d) Hydrologic *S*. Scale is nonlinear.

[29] Figure 3a shows the annual mean dust burden simulated using the Uniform erodibility factor. The differences in the absolute column burden among the erodibility hypotheses are hard to discern. Differences due to regional geomorphic influence appear near all dust source regions. All three experiments (Figures 3b, 3c, and 3d) show enhanced burdens downwind of the Bodele depression, the strongest dust source seen in TOMS AAI observations [*Prospero et al.*, 2002]. Figures 3b, 3c, and 3d also show enhanced dustiness near the Chotts of Tunisia and northeast Algeria, and Mali near Tombouctou, and the Tarim Basin in China and Lake Eyre Playa in Australia. Reduced dustiness is common to the experiments in the central and western Sahara, Arabian Sea, and Western Australia regions. These changes relative to the Uniform hypothesis are generally realistic on the basis of previous TOMS AAI interpretations. This regional behavior is consistent with the hypothesis that hydrologic basins are richer in dust source materials, and thus more efficient dust sources than nearby regions with comparable meteorology but less erodible source material. (More detailed discussions of the results in the important source regions of North Africa, East Asia, and Australia follow Figure 5.)

[30] The hypotheses with spatially varying erodibility reduce the burden over the north Indian Ocean, where mineral dust concentrations are highly uncertain [*Prospero*, 1996]. However recent experiments indicate dust may be less important than previously thought [*Rasch et al.*, 2001]. The Hydrologic experiment predicts the greatest burden from sources in the Thar Desert in the Indus river valley region between India and Pakistan.

[31] The differences between the Topographic and Uniform hypotheses show the important impact that topography has on emissions. Assigning enhanced erodibility to topographic minima [*Ginoux et al.*, 2001] realistically increases emissions in the central Sahara around the Bodele depression, the Tarim Pendi (Tarim Basin) and Gobi Desert regions of China, the Aral Sea region, the southern flanks of Himalayas, the and the Lake Eyre region in central Australia. Emissions are reduced in the eastern Sahara near Sudan, in Namibia, in South America near Patagonia, and in Western Australia.

[32] The differences between the Geomorphic and Topographic hypotheses show the impact of realistically defined sedimentary basins. Geomorphic basins enhance burdens near the Bodele Depression, Namibia, the Aral Sea, Western Australia, and reduce emissions from the Algerian and Malian regions of the western Sahara. Of the four erodibility hypotheses tested, the Geomorphic and Topographic produced the closest overall agreement with observations.

[33] The differences between the Hydrologic and Geomorphic hypotheses show the regions in which present-day hydrological transport and disturbances would be expected to have the greatest impact. Regions with increased emissions include the Bodele Depression, the Indus River valley in Pakistan, and the Mesopotamian region in Iraq. Each of these regions has a high concentration of sediments from the upstream regions it drains. The Hydrologic erodibility *S* is much larger in active river valleys than in desert basins, so it is somewhat surprising that the simulated dust distribution is not completely dominated by Earth's major coastal estuaries in the Hydrologic case. This is because other constraints in the dust model [*Zender et al.*, 2003], primarily

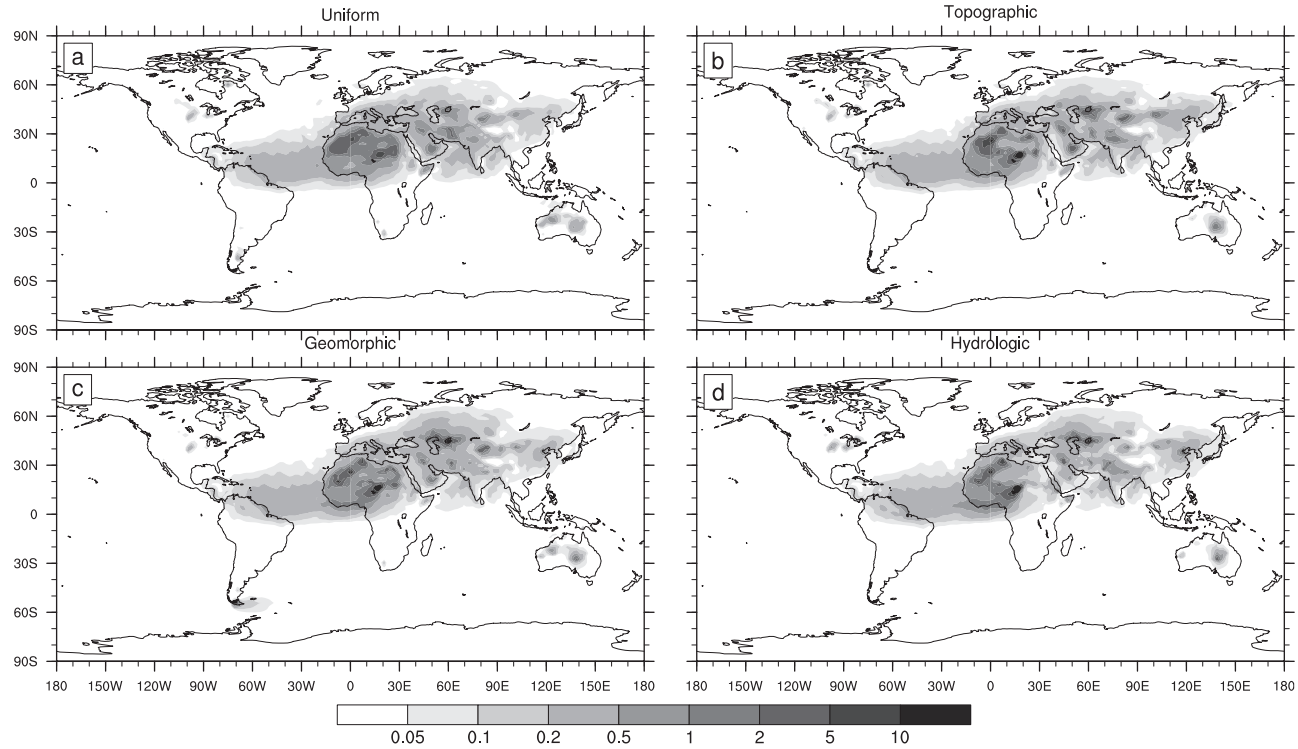

Figure 4. Predicted annual mean mass deposition flux [$\mu g\ m^{-2}\ s^{-1}$] for (a) Uniform S, (b) Topographic S, (c) Geomorphic S, and (d) Hydrologic S. Scale is logarithmic.

vegetation and soil moisture, control dust emissions in regions hospitable to vegetation.

[34] Regions where the present-day Hydrologic hypothesis decreases emissions relative to the Geomorphic hypothesis include the Aral Sea region, the Tarim Basin, the eastern Sahara, and Patagonia. These regions are known dust sources [*Prospero et al.*, 2002], and we should continue to examine whether the present-day Hydrologic hypothesis improves model performance in them by using improved in situ and satellite observations.

[35] Figure 4 shows the annual mean deposition flux [$\mu g\ m^{-2}\ s^{-1}$] for each erodibility hypothesis. Deposition closely follows mobilization (Figure 2) because the large particles which dominate the mobilization mass budget fall near the source region. As expected the differences among deposition patterns diminish with distance from the source regions so that the patterns of long range transport are very similar. We compare these deposition data to station observations in section 3.4.2.

[36] The Uniform deposition structure appears only slightly more diffuse than the deposition structure in the spatially heterogeneous cases. This is due to intrinsic spatial heterogeneity in the bioclimatic controls on dust emissions and deposition: winds, vegetation, soil texture, and moisture. By our definition, the erodibility S alters the gradient of source strength (and thus deposition) in existing source regions, but it cannot create entirely new source (or sink) regions.

3.2. Mass Budget Sensitivity

[37] The erodibility factors each have a distinct effect on the global mass budget of simulated dust. Table 1 compares the annual mean dust budget of the control to the three experiments. As mentioned previously, all experiments were normalized a posteriori to achieve the same global burden, 19.3 Tg. Measurements of the global mass fluxes or lifetime of dust do not exist. Estimates of these quantities vary by as much as a factor of two among models [*Penner et al.*, 2001; *Zender et al.*, 2003]. In DEAD, these quantities vary by 10–20% for a given global burden, depending on the erodibility factor.

[38] The lifetime of dust in the Geomorphic and Hydrologic experiments is ~10–20% shorter than in the Topographic and Uniform cases because the emission regions of the first two experiments are slightly closer to hydrologically active regions where wet deposition is significant. However, the relative roles of wet and dry deposition do not vary by more than a few percent among all the cases so the main effect of shorter lifetime is to intensify the lifecycle of dust, rather than to repartition the mass budget.

3.3. Comparison to TOMS AAI

[39] We now use the climatological averages of the three independent data sets described in sections 2.2–2.3 to quantify the efficacy of each hypothesis. First we compared

Table 1. Climatological Budget Statistics

Quantity	Uniform	Topo	Geo	Hydro
Burden[a]	19.3	19.3	19.3	19.3
Emission[b]	1438	1535	1638	1632
Lifetime[c]	5.0	4.7	4.4	4.4
Global τ[d]	0.033	0.034	0.034	0.034

[a]Prescribed atmospheric burden in Tg.
[b]Emissions of $D < 10$ μm particles in Tg yr^{-1}.
[c]Turnover time in days.
[d]Optical depth at 0.63 μm.

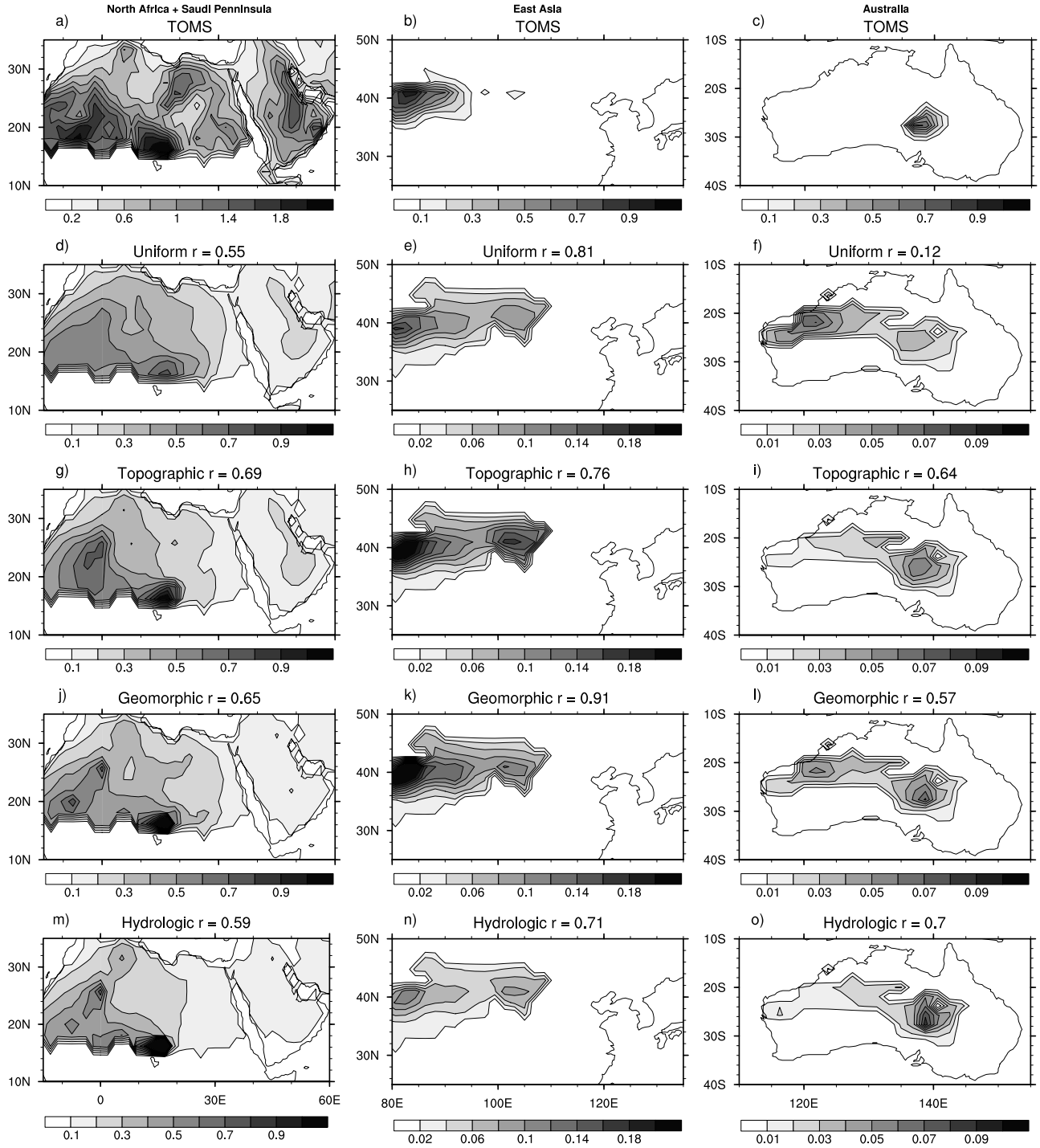

Figure 5. Mean 1980–2001 TOMS AAI and predicted dust AOD for 1990–1992 in the Saharan desert and Saudi Arabian peninsula (first column), East Asia (second column), and Australia (third column). (a–c) TOMS AAI, (d–f) Uniform *S*, (g–i) Topographic *S*, (j–l) Geomorphic *S*, (m–o) Hydrologic *S*. *r* is the spatial correlation coefficient between the experiment and TOMS AAI.

model-simulated AOD to the TOMS-observed AAI and AOD in three important desert regions. The regions and their boundaries are (1) Sahara and the Saudi Arabian Peninsula, (10–35°N, −20–60°E); (2) EastAsia, (25–50°N, 80–135°E); (3) Australia (45–10°S, 110–160°E). We expect predicted dust AOD to vary linearly with TOMS AAI in dust-dominated regions [*Chiapello et al.*, 1999; *Hsu et al.*, 1999]. The procedure for comparing the observed to predicted spatial distributions in these source regions was as follows. First we re-binned TOMS AAI and AOD from $1^\circ \times 1.25^\circ$ and $1^\circ \times 1^\circ$ grids, respectively, to the coarser, T62-resolution model grid (approximately $2^\circ \times 2^\circ$). Data from ocean cells and cells with mean annual vegetation $V > 0.3$ m^2 m^{-2} [*Kergoat et al.*, 1999; *Zender et al.*, 2003]

were then removed. Most of Australia outside the Lake Eyre Playa does not pass this vegetation criteria so we used $V > 0.5$ m^2 m^{-2} in Australia.

[40] Figure 5 shows the observed and predicted spatial distribution of aerosols over the resulting potential source regions in the Sahara+Arabian Peninsula, East Asia, and Australia. In the Sahara+Saudi Arabia region, the Uniform experiment (Figure 5d) appears too diffuse in the west and north Sahara relative to the central Central African region near Lake Chad. Dust emissions are also too diffuse in the south and eastern Saudi Arabian Peninsula relative to TOMS (Figure 5a). The Topographic erodibility S (Figure 5g) captures more of the observed structure of the west and central Sahara than the other experiments. However, the west Saharan sources are centered too far North, and with too little north–south structure. The Geomorphic S (Figure 5j) underestimates the relative importance of the western Sahara region, but appears to capture the north–south structure better than the other experiments. In particular the source near Tombouctou (18–20N, 8–10W) is captured, as is some of the SW-to-NE structure in the Eastern Libyan Desert.

[41] To remove any contribution of carbonaceous aerosol from biomass burning that might contaminate the TOMS data in the Sahara+Saudi Arabia region, we performed the same analysis after removing the peak months of Sahelian burning (December–February, DJF) from all data. This reduces the spatial correlations r between the models and TOMS AAI in the region by 0.16 (Uniform), 0.17 (Topographic), 0.15 (Geomorphic), and 0.12 (Hydrologic) to 0.39, 0.52, 0.50, and 0.47, respectively. These correlations are all highly statistically significant. This is consistent with the models simulating regional dust sources better in DJF than March–November, regional TOMS data being significantly influenced by biomass burning coincident with real dust sources, and/or the models getting the source regions correct but the DJF seasonality incorrect. In any case there is no qualitative difference with the analysis and ranking based on the full 12 month climatology.

[42] The dominant feature in TOMS AAI in East Asia (Figure 5b) is the Tarim Basin. The AAI in the Gobi Desert is 5–10 times weaker. However, *Prospero et al.* [2002] emphasize that TOMS AAI does not detect all sources, and that emissions from the Gobi region appear to be increasing. They note that Gobi dust sources may be activated by spring fronts whose clouds hamper the TOMS aerosol detection. Compared to TOMS AAI, all our simulations exaggerate the relative importance of the Gobi Desert. With the Uniform and Hydrologic experiments (Figures 5e and 5n), the Tarim Basin AOD is less than twice the Gobi AOD. The Topographic erodibility (Figure 5h) yields the largest AOD in the Gobi. The Geomorphic erodibility (Figure 5k) best balances source strength and location.

[43] To isolate the signal from springtime Asian dust sources, we performed the same analysis using only the months of maximum dust activity in that region (March–May, MAM), which increases the prominence of dust sources east of 100°E in the TOMS AAI and in all the models. This reduces the spatial correlations r between the models and TOMS AAI in the region by +0.06 (Uniform), +0.12 (Topographic), −0.01 (Geomorphic), and +0.01 (Hydrologic) to 0.87, 0.89, 0.90, and 0.72, respectively. The Uniform and Topographic models perform significantly better when only MAM is considered. This is consistent with the Uniform and Topographic models simulating dust in East Asia better in MAM than in June–February. Moreover, the spatial distribution of East Asian dust in the Topographic model is virtually indistinguishable from the Geomorphic model in MAM. In contrast to the Topograhic model, however, the Geomorphic model also captures the correct relative magnitude of Spring versus Fall surface dust concentration at Jeju Island, Korea (see Figure 6 below). Since MAM accounts for only about 40% of annual surface dust at Jeju, it is important to evaluate East Asian model performance based on the whole year.

[44] The erodibility hypotheses clearly differentiate themselves in Australia. TOMS AAI (Figure 5c) shows that the main Australian dust source region is the Lake Eyre Basin [*Prospero et al.*, 2002]. The Uniform erodibility hypothesis (Figure 5f) predicts strong emissions and burdens from the Great Sandy Desert in northwestern Australia. The three spatially varying erodibility hypotheses reproduce this feature (Figures 5i, 5l, and 5o), most clearly in the Topographic case (compare Figure 3b). The Geomorphic (Figure 5l), and to a lesser extent, the Hydrologic hypothesis (Figure 5o), predict a secondary maximum emanating from the Great Sandy Desert to the Hammersley range to the west. This feature is not observed in TOMS AAI imagery (Figure 5c), although the regional Dust Storm Index of *McTainsh* [1998] shows strong sources near Carnarvon and Port Hedland in this region.

[45] The linear correlation coefficient r of the spatial distribution of dust in each simulation with TOMS AAI appears at the top of each panel in Figure 5. Table 2 summarizes these r-values, along with the value of r computed using the TOMS AOD data set. The number N of valid (land, vegetation < 0.3 m^2 m^{-2}) T62 grid points used in these comparisons is 290, 77, and 59, respectively. With the sole exception is the Uniform case in Australia ($r = 0.12$), the spatial correlations between all the models and the TOMS AAI are highly significant ($p < 0.005$), even if we assign only 1/3 degree of freedom per grid point. Correlations with TOMS AAI are generally significantly better than with TOMS AOD. This might be expected since AOD observations include nondust aerosols whereas the simulations predict only mineral dust. However, the greatest difference between the AAI and AOD spatial structures are in Africa, not in Asia. This is paradoxical since East Asia has significant anthropogenic sulfate and carbonaceous aerosol all year, but Saharan Africa appears to be dominated by mineral dust all year [*Tegen et al.*, 1997; *Chin et al.*, 2002]. This may be partially reconciled by examining the dust aerosol height assumed in the look-up tables used to retrieve TOMS AOD from two UV radiances. This height comes from GOCART model simulations [*Ginoux et al.*, 2001; *Torres et al.*, 2002]. DEAD (and other models) may compare less favorably to TOMS AOD where it predicts dust at a different height from GOCART.

[46] We also compared our model results to the TOMS climatology assembled just from the simulation period of 1990–1992. These 3 years contain only about one-sixth of the available TOMS AAI data. In the African region, comparing 1990–1992 model simulations to 1990–1992 TOMS AAI reduces the spatial correlations in Table 2 by

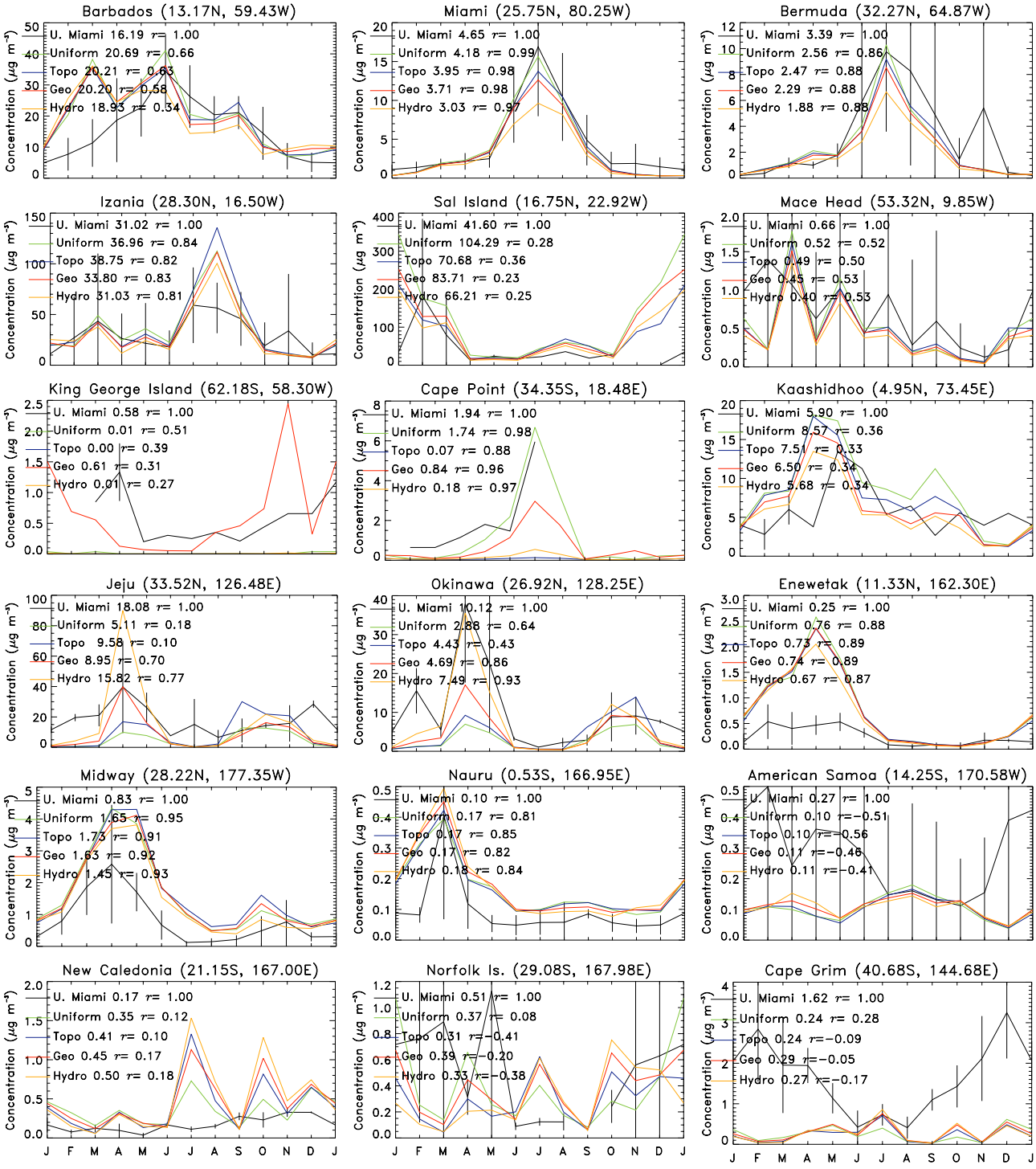

Figure 6. Predicted (colors) and observed (black) monthly mean surface dust concentration [μg m^{-3}] at University of Miami stations. Black whiskers show 2 standard deviations for observed values. No whisker indicates data only available for same month in $N < 2$ years. Legend names are followed by the climatological mean concentration [μg m^{-3}] and the linear correlation coefficient r with the observed monthly mean data.

0.10 (Uniform), 0.09 (Topographic), 0.08 (Geomorphic), and 0.07 (Hydrologic). The resulting correlations are 0.45, 0.60, 0.57, and 0.52, respectively. Thus all models predict the spatial structure of dust in this region more poorly (and by a nearly uniform degree) when compared to 1990–1992 than to 1980–2001. This suggests that some sources in this region in the models are under-sensitive to interannual variations in meteorology. In East Asia, comparing to only 1990–1992 TOMS data changes the spatial correlations by +0.01 (Uniform), +0.01 (Topographic), −0.01 (Geomorphic), and +0.01 (Hydrologic). Thus 1990–1992 closely represents the 22-year TOMS AAI record in Asia. In

Table 2. Spatial Correlation of Model AOD with TOMS AAI and AOD[a]

	Sahara			East Asia			Australia		
Hypothesis	AAI	AOD	r^{2b}	AAI	AOD	r^2	AAI	AOD	r^2
Uniform	0.55	0.18	0.30	0.81	0.78	0.66	0.12	0.27	0.01
Topographic	**0.69**	0.34	0.47	0.76	0.70	0.58	0.64	0.55	0.41
Geomorphic	0.65	0.37	0.42	**0.91**	0.77	0.83	0.57	0.32	0.32
Hydrologic	0.59	0.43	0.35	0.71	0.67	0.50	**0.70**	0.51	0.49

[a]Number N of valid T62 grid points is 290, 77, and 59 for Saharan, East Asian, and Australian regions, respectively. Highest r for TOMS AAI in each region is boldfaced.
[b]Fraction of observed (AAI) spatial structure explained by model, computed as r^2_{AAI}.

Australia, comparing to only 1990–1992 TOMS data changes the spatial correlations by +0.10 (Uniform), −0.01 (Topographic), −0.11 (Geomorphic), and +0.00 (Hydrologic). The resulting correlations are 0.22, 0.63, 0.46, and 0.70, respectively. Thus the model rankings obtained from comparisons to 1990–1992 AAI agree with those obtained from 1980–2001 AAI comparisons in all three regions.

[47] The square of the spatial correlations may be interpreted as the fraction of the spatial variance (i.e., structure) explained by the model. Table 2 shows the spatial variance in the TOMS AAI observations explained by each model (r^2). The three hypotheses with spatially heterogeneous erodibility factors match the spatial structure of TOMS AAI better than the Uniform erodibility, which performs worst in Africa and Australia (Figures 5d and 5f). The best performance in Africa, East Asia, and Australia is achieved by the Topographic, Geomorphic, and Hydrologic erodibility, which explain 47%, 83%, and 49% of the observed spatial structure, respectively (Figures 5g, 5k, and 5o).

[48] Figure 5 and Table 2 show that different erodibility hypotheses may prevail in different regions. We estimated the range of spatial variability explained by heterogeneous erodibility by subtracting r^2 from the Uniform case from the r^2 of the heterogeneous hypotheses in each region. Using Uniform erodibility as a baseline in this way, we estimate that heterogeneous S explains up to an additional 15–20%, 15–20%, and 50% of the spatial structure of dust emissions in Sahara+Arabian Peninsula, East Asia, and Australia, respectively.

3.4. Comparison to Station Data

[49] It is important to consider the fidelity of the model performance against direct station measurements of dust concentration and deposition. The number of such stations is few: 19 stations for concentration and 11 for deposition. However, stations remote from dust source regions are representative of dust concentration and deposition over large spatial regions [*Mahowald et al.*, 2003]. We evaluate model performance against station measurements of concentration and deposition using five statistics. Each statistic is computed with both raw and logarithmically transformed data. The root-mean square (RMS) absolute error $\mathrm{RMS_{abs}}$ is computed as

$$\mathrm{RMS_{abs}} = \sqrt{\frac{1}{N}\sum_{i=1}^{N}(x_i - y_i)^2} \tag{3}$$

where x_i are observed data and y_i are modeled data, or the natural logarithms thereof. Thus $\mathrm{RMS_{abs}}$ is a strict measure of absolute model bias against the observed dust concentration and deposition measurements. The stations with the greatest absolute dust concentrations and fluxes dominate $\mathrm{RMS_{abs}}$ when it is computed using untransformed (linear) data. Therefore we also compute $\mathrm{RMS_{abs}}$ with logarithmically transformed data, i.e., using $\log x$ and $\log y$ in place of x and y in equation (3). The advantage of the logarithmic $\mathrm{RMS_{abs}}$ is that it weights absolute biases at stations with smaller concentrations and fluxes approximately equally to dustier stations. The final statistic we examined is the relative root-mean square bias, $\mathrm{RMS_{rel}}$. $\mathrm{RMS_{rel}}$ is computed from the relative, rather than absolute, bias at each station

$$\mathrm{RMS_{rel}} = \sqrt{\frac{1}{N}\sum_{i=1}^{N}\left(\frac{x_i - y_i}{x_i}\right)^2} \tag{4}$$

Thus $\mathrm{RMS_{rel}}$ measures the factor by which the model simulation is in error at each station. We show $\mathrm{RMS_{rel}}$ computed with transformed (logarithmic) data for completeness, although its interpretation is problematic.

3.4.1. Comparison to University of Miami Concentration

[50] The climatological mean dust concentrations [$\mu g\ m^{-3}$] observed at 19 University of Miami stations and predicted in the model are scatterplotted in Figure 7. On these logarithmic axes, the spread in model values for the various erodibility factors does not appear large. The greatest intermodel spread [%] occurs for stations in and downwind of source regions, including Sal Island (57%) and Cape Point (2500%) which sample African sources, Kaashidhoo (50%) which samples sources regions surrounding the north Indian Ocean, and Jeju (310%) and Okinawa (280%) which sample far East Asian dust. The intermodel differences at Barbados (9%), Miami (38%), and Bermuda (36%) are relatively small. This indicates that diffusive processes mix African dust significantly during transport across the Atlantic, reducing the sensitivity of these stations to the exact geographic distribution of sources upwind.

[51] Intermodel spread was minimal at most nondusty stations, including Mace Head (30%) in the North Atlantic, Oahu (20%), Midway (19%), and Enewetak (13%) in the North Pacific, and Nauru (6%), American Samoa (10%), Norfolk Is. (26%), and Cape Grim (21%) in the South Pacific. Model performance at these nondusty regions is important since these regions cover a large portion of the globe and over-prediction of dust in remote regions could severely bias global mass fluxes and radiative forcing of dust.

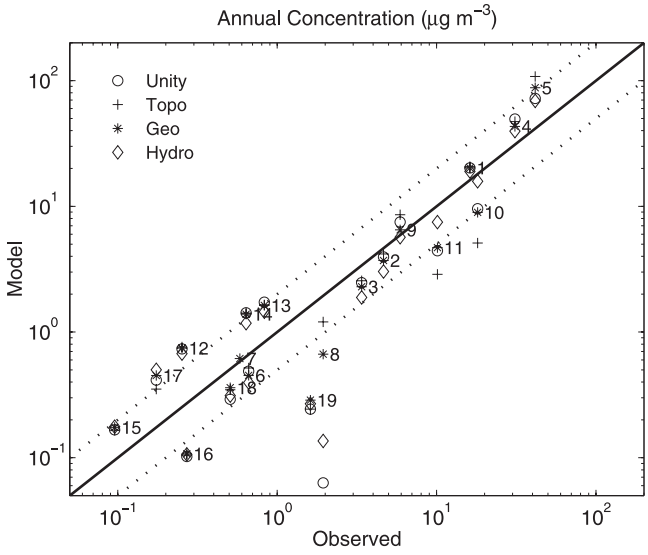

Figure 7. Predicted and observed climatological mean surface concentration of dust in μg m^{-3} at University of Miami stations. Dashed lines indicate factor of two disparity. Site numbers are as follows: 1. Barbados, 2. Miami, 3. Bermuda, 4. Izaña, 5. Sal Island, 6. Mace Head, 7. King George Island, 8. Cape Point, 9. Kaashidhoo, 10. Jeju, 11. Okinawa, 12. Enewetak, 13. Midway, 14. Oahu, 15. Nauru, 16. American Samoa, 17. New Caledonia, 18. Norfolk Island, and 19. Cape Grim. Axes are logarithmic.

[52] We also examined the fidelity of the mean seasonal cycle of concentration predicted using each erodibility factor. Figure 6 compares predicted to observed monthly mean dust concentrations in μg m^{-3}.

[53] The monthly intermodel differences are of course often greater than the annual mean intermodel differences (Figure 7). The seasonal cycles at most remote stations are not very sensitive to erodibility, and remain close to the 1990s mean seasonal cycle for the Geomorphic case shown in Figure 6 of *Zender et al.* [2003]. However, S appears to strongly affect the seasonality and strength of sources in East Asia, Patagonia, and South Africa. At Jeju Island, near Korea, and Okinawa, which sample Asian outflow, the dust concentration in Spring is realistically larger than that in the Fall only in the Geomorphic and Hydrologic cases. The Geomorphic erodibility greatly improves the mean and seasonal cycle simulation at both King George Island and Cape Point, apparently because of enhanced emissions from Patagonia and South Africa, respectively.

[54] *Luo et al.* [2003] show that intermodel differences between DEAD and GOCART [*Ginoux et al.*, 2001] in East Asia and downwind of Australia are strongly sensitive to biases in surface meteorology. Our results show that erodibility also plays a significant role in these regions.

[55] Table 3 summarizes the statistical correlations of each erodibility simulation with the annual mean University of Miami station data shown in Figure 7. The linear correlation r exceeds 0.9 for all erodibility factors. The Hydrologic erodibility produces the slope m and offset b of the surface concentration regression closest to 1 and to 0, respectively. The Hydrologic simulation also has the smallest RMS errors, both absolute and relative. However, these linear metrics are dominated by model performance in the dusty subtropical north Atlantic. The logarithmic statistics more evenly weight dusty and nondusty regions. The Geomorphic S produces significantly better logarithmic correlation, offset, and RMS statistics than the other simulations. Overall the Geomorphic and Hydrologic erodibility best reproduce the station concentration data.

3.4.2. Comparison to Surface Deposition

[56] Figure 8 compares the 1990–1992 mean model predictions of dust deposition [g m^{-2} yr^{-1}] with observations from 11 stations compiled by *Ginoux et al.* [2001]. The intermodel spread is greatest at the two dustiest stations, in the Takla Makan Desert and near Tel Aviv. The Geomorphic case is significantly closer to observations in the Takla Makan than the others. This is consistent with the superior spatial structure of the Geomorphic case in Asia shown in section 3.3. At the more remote stations, the intermodel differences are always less than 40%. Table 4 summarizes the statistical correlations of each experiment with the 11 stations in the observed climatology shown in Figure 8.

[57] The linear correlation r is near 1.0 for all erodibility factors. This is due to the huge dominance of the Takla Makan data point, where deposition exceeded the sum of the deposition at the other stations by a factor of ~20. Neglecting the Takla Makan point reduces the linear r to 0.74, 0.75, 0.79, and 0.52 for the Uniform, Topographic, Geomorphic, and Hydrologic cases, respectively. The Geomorphic simulation has the best slope, offset, and RMS errors for both the linear and logarithmic statistics. The same is true if the Takla Makan point is discarded. Thus the Geomorphic erodibility factor appears to offer a significant advantage in predicting global dust deposition. Because the of the small number of stations, none of which are directly downwind of the important North

Table 3. Biases in Simulation of Annual Mean Concentration at 19 University of Miami Stations[a]

	Linear[b]					Logarithmic[c]				
Hypothesis	r	m	b	RMS_{abs}	RMS_{rel}	r	m	b	RMS_{abs}	RMS_{rel}
Uniform	0.91	2.04	−4.01	16.06	0.88	0.84	**1.00**	−0.11	0.52	2.12
Topographic	0.96	1.58	−2.30	8.60	0.85	0.78	1.03	−0.20	0.68	2.80
Geomorphic	0.94	1.74	−2.96	11.28	0.83	**0.91**	0.93	**0.00**	**0.33**	**1.35**
Hydrologic	**0.98**	**1.47**	**−1.97**	**6.71**	**0.81**	0.81	1.03	−0.18	0.60	2.46

[a]Value of best metric in each category is boldfaced.
[b]Linear correlation coefficient r and best fit parameters to $y = m\,x + b$ where x are observed data and y are simulated. RMS defined in equations (3) and (4).
[c]Statistics computed using log x and log y in place of x and y.

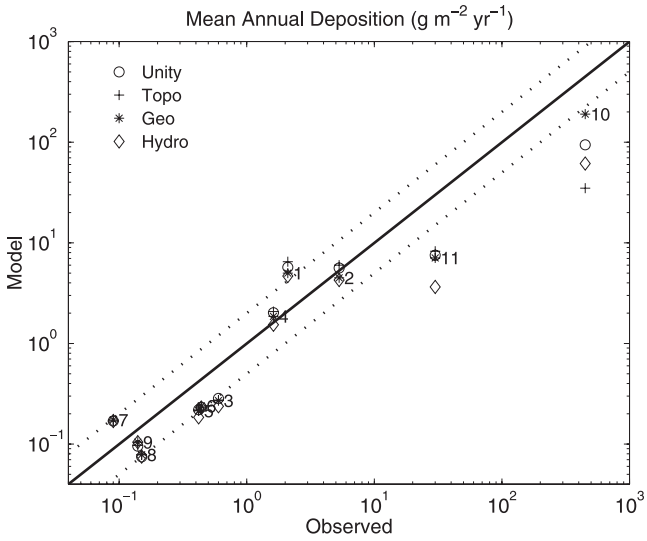

Figure 8. Predicted and observed climatological mean dust deposition flux in g m^{-2} yr^{-1} at 11 stations compiled by *Ginoux et al.* [2001]. Site numbers are as follows: 1. French Alps (45.5N, 6.5E), 2. Spain (41.8N, 2.3E), 3. Midway (28.2N, 177.35W), 4. Miami (25.75N, 80.25W), 5. Oahu (21.3N, 157.6W), 6. Enewetak (11.3N, 162.3E), 7. Fanning (3.9N, 159.3W), 8. Samoa (14.25S, 170.6W), 9. New Zealand (34.5S, 172.75E), 10. Takla Makan (40.0N, 85.0E), and 11. Tel Aviv (32.0N, 34.5E). Axes are logarithmic.

African dust plume, we should not extrapolate this result globally.

4. Conclusions

[58] We investigated whether and how spatial heterogeneity of soil erodibility depends on regional topography, geomorphology, and hydrology. Because climatological measurements of global dust emissions are not available, we evaluated four distinct erodibility hypotheses by implementing them in a global tracer transport model driven by observed winds. We compared the results to three different data sets. Significant intermodel differences appeared in all important source regions, and in all three data sets. Since all differences in the model simulations are attributable to soil erodibility hypotheses, we presume that the hypothesis producing the smallest disparity with observations is the most realistic. In almost all cases the incorporation of regional topographic, geomorphic, and hydrologic influences improves the dust simulations. Our main conclusion is that local erodibility is demonstrably sensitive to regional geomorphic and hydrologic processes.

[59] Comparison to TOMS AAI showed the Topographic, Geomorphic, and Hydrologic hypotheses performed best in the North African, East Asian, and Australian source regions, respectively. In the majority of areas the Uniform erodibility produced the worst agreement with the spatial structure of TOMS AAI. The Uniform erodibility performed best in East Asia in comparison to TOMS AOD, which is a less reliable metric for dust than AAI. The Uniform hypothesis explains none of the spatial structure of emissions in Australia. Australian emissions are strongly consistent (30–50% of spatial structure explained) with spatially heterogeneous erodibility hypotheses.

[60] We intercompared model simulations with seasonal and annual mean dust concentration measurements from 19 worldwide stations operated by the University of Miami. Distinctions among the erodibility factors were largest near source regions, with concentrations differing among models by less than 20% at most remote stations. The Hydrologic or Geomorphic erodibility assumption compared best to observations, depending on which statistic was used. Using linear statistics, which favor performance in regions of high dust concentration, the Hydrologic erodibility performed best and the Topographic and Geomorphic erodibility performed nearly as well. Using logarithmic statistics, which more evenly weight performance in dusty and nondusty regions, the Geomorphic erodibility performed significantly better than the others. The Geomorphic S also performed best in every metric when compared to 11 climatological station observations of dust mass deposition flux. However, the deposition evaluation does not reflect performance globally because none of the stations are located directly downwind of the strong north African dust plume.

[61] The Topographic erodibility factor Equation (2) is a resolution-dependent parameterization with no underlying physical basis for its algebraic form. However, subgrid-scale problems are endemic to large-scale models of nonlinear processes. The Topographic S suffers from unresolved topography and discontinuity, while the Geomorphic and Hydrologic S suffer from discretization of topography and flow direction. Nevertheless, our physically based erodibility factors ameliorate the subgrid-scale problem in at least one way. In contrast to the Topographic S, the Geomorphic and Hydrologic S converge with increasing model resolution.

[62] Because the Geomorphic erodibility performs nearly as well or better than the other erodibility factors in most metrics, we infer that it most closely represents realistic erodibility on Earth. For this reason, we now use the Geomorphic S globally in the DEAD model [*Zender et al.*, 2003] although competing erodibility hypotheses perform nearly

Table 4. Biases in Simulation of Annual Mean Deposition at 11 Stations[a]

	Linear[b]					Logarithmic[c]				
Hypothesis	r	m	b	RMS_{abs}	RMS_{rel}	r	m	b	RMS_{abs}	RMS_{rel}
Uniform	0.97	0.07	2.06	125.34	0.84	0.93	0.77	−0.15	0.45	0.78
Topographic	**1.00**	0.21	1.35	107.52	0.74	0.95	0.85	**−0.14**	0.37	0.73
Geomorphic	**1.00**	**0.42**	**0.26**	**78.66**	**0.66**	**0.96**	**0.90**	**−0.14**	**0.32**	**0.71**
Hydrologic	**1.00**	0.13	0.97	117.44	0.68	0.94	0.78	−0.21	0.45	0.78

[a]Value of best metric in each category is boldfaced.
[b]Linear correlation coefficient r and best fit parameters to $y = m\,x + b$ where x are observed data and y are simulated.
[c]Statistics computed using log x and log y in place of x and y.

as well or better in certain regions. All our results were obtained with a specific dust physics model (DEAD), transport model (MATCH), and set of boundary conditions (NCEP). It would be interesting to establish the generality of our results by testing our hypotheses in different model frameworks.

[63] A Hydrologic erodibility S representing the most recent moist climate in each source region (e.g., the mid-Holocene in the Sahara) might be significantly better than the present-day runoff S studied here. We speculate that the Geomorphic erodibility performs well because it implicitly represents the potential sediment accumulation which could have occurred in past moist climates. Improved representation of the pedogenic, geomorphic, and hydrologic history of source regions is likely to improve global-scale and mesoscale dust forecasting.

[64] One goal of improving understanding and representation of erodibility is to help discriminate between natural and anthropogenic soil emissions. Our erodibility factors only attempt to parameterize natural processes and features relevant to sediment accumulation and disturbance. Mahowald et al. (submitted manuscript, 2003) argue that the topographic erodibility S may implicitly represent some anthropogenic contribution to erodibility because human settlements and agricultural activity are preferentially located near available water, i.e., in topographic depressions. This argument applies even more strongly to the Geomorphic and Hydrologic erodibility factors. The dust observations against which we compare do not discriminate between natural and anthropogenic dust. Thus some of the bias between our simulations and the observations could be due to anthropogenic contributions (e.g., disturbance) to erodibility that are not represented. Only continued monitoring and evaluation of soil erodibility and dust emissions will allow us to make the fine distinctions between natural and anthropogenic dust. By providing a physically based framework for determining and comparing erodibility factors, the present work is a step in this direction.

[65] **Acknowledgments.** We thank J. Famiglietti for assistance with hydrological computations, P. Ginoux for providing his topographic erodibility factor, S. Levis for guidance with land surface parameterizations, N. Mahowald for constructive and insightful comments, G. McTainsh for helpful discussions on erodibility, and R. Arimoto, J. Prospero, and D. Savoie for providing data to improve and evaluate the model. Suggestions by three anonymous reviewers greatly improved the quality of the final manuscript. This research was supported in part by NASA grants NAG5-10147 and NAG5-10546.

References

Alfaro, S. C., A. Gaudichet, L. Gomes, and M. Maillé, Modeling the size distribution of a soil aerosol produced by sandblasting, *J. Geophys. Res.*, *102*, 11,239–11,249, 1997.

Bonan, G. B., A land surface model (LSM version 1.0) for ecological, hydrological, and atmospheric studies: Technical description and user's guide, *Tech. Rep. NCAR TN-417 + STR*, Natl. Cent. for Atmos. Res., Boulder, Colo., 1996.

Bonan, G. B., S. Levis, L. Kergoat, and K. W. Oleson, Landscapes as patches of plant functional types: An integrating concept for climate and ecosystem models, *Global Biogeochem. Cycles*, *16*(2), 1021, doi:10.1029/2000GB001360, 2002.

Chiapello, I., J. M. Prospero, J. R. Herman, and N. C. Hsu, Detection of mineral dust over the North Atlantic Ocean and Africa with the Nimbus 7 TOMS, *J. Geophys. Res.*, *104*, 9277–9291, 1999.

Chin, M., et al., Tropospheric aerosol optical thickness from the GOCART model and comparisons with satellite and sun photometer measurements, *J. Atmos. Sci.*, *59*, 461–483, 2002.

D'Almeida, G. A., On the variability of desert aerosol radiative characteristics, *J. Geophys. Res.*, *92*, 3017–3026, 1987.

Fécan, F., B. Marticorena, and G. Bergametti, Parametrization of the increase of the aeolian erosion threshold wind friction velocity due to soil moisture for arid and semi-arid areas, *Ann. Geophys.*, *17*, 149–157, 1999.

Gillette, D., A wind tunnel simulation of the erosion of soil: Effect of soil texture, sandblasting, wind speed, and soil consolidation on dust production, *Atmos. Environ.*, *12*, 1735–1743, 1978.

Gillette, D. A., A qualitative geophysical explanation for "hot spot" dust emitting source regions, *Beitr. Phys. Atmos.*, *72*, 67–77, 1999.

Gillette, D. A., B. Marticorena, and G. Bergametti, Change in the aerodynamic roughness height by saltating grains: Experimental assessment, test of theory, and operational parameterization, *J. Geophys. Res.*, *103*, 6203–6209, 1998.

Ginoux, P., M. Chin, I. Tegen, J. Prospero, B. Holben, O. Dubovik, and S.-J. Lin, Sources and distributions of dust aerosols simulated with the GOCART model, *J. Geophys. Res.*, *106*, 20,273–20,555, 2001.

Graham, S. T., J. S. Famiglietti, and D. R. Maidment, Five minute, 1/2° and 1° data sets of continental watersheds and river networks for use in regional and global hydrologic and climate system modeling studies, *Water Resour. Res.*, *35*, 583–587, 1999.

Herman, J. R., P. K. Bhartia, O. Torres, C. Hsu, C. Seftor, and E. Celarier, Global distribution of UV-absorbing aerosols from Nimbus 7/TOMS data, *J. Geophys. Res.*, *102*, 16,911–16,922, 1997.

Hsu, N. C., J. R. Herman, O. Torres, B. N. Holben, D. Tanré, T. F. Eck, A. Smirnov, B. Chatenet, and F. Lavenu, Comparisons of the TOMS aerosol index with Sun-photometer aerosol optical thickness: Results and applications, *J. Geophys. Res.*, *104*, 6269–6279, 1999.

Iversen, J. D., and B. R. White, Saltation threshold on Earth, Mars, and Venus, *Sedimentology*, *29*, 111–119, 1982.

Jenson, S. K., and J. O. Domingue, Extracting topographic structure from digital elevation data for geographic information system analysis, *Photogramm. Eng. Remote Sens.*, *54*, 1593–1600, 1988.

Kalnay, E., The NCEP/NCAR 40-year reanalysis project, *Bull. Am. Meteorol. Soc.*, *77*, 437–471, 1996.

Kergoat, L., S. Moulin, P. Cayrol, and G. Dedieu, Controlling vegetation growth models with satellite measurements, in *Advances in Environmental and Ecological Modelling*, edited by F. Blasco and A. Weill, pp. 73–89, Elsevier Sci., New York, 1999.

Luo, C., N. M. Mahowald, and J. del Corral, Sensitivity study of meteorological parameters on mineral aerosol mobilization, transport, and distribution, *J. Geophys.*, *108*, doi:10.1029/2002JD003483, 2003.

Mahowald, N. M., C. S. Zender, C. Luo, D. Savoie, O. Torres, and J. del Corral, Understanding the 30 year Barbados desert dust record, *J. Geophys. Res.*, *107*(D21), 4561, doi:10.1029/2002JD002097, 2002.

Mahowald, N. M., C. Luo, J. del Corral, and C. S. Zender, Interannual variability in atmospheric mineral aerosols from a 22-year model simulation and observational data, *J. Geophys.*, *108*(D12), 4352, doi:10.1029/2002JD002821, 2003.

Maring, H., D. L. Savoie, M. A. Izaguirre, C. McCormick, R. Arimoto, J. M. Prospero, and C. Pilinis, Aerosol physical and optical properties and their relationship to aerosol composition in the free troposphere at Izaña, Tenerife, Canary Islands during July 1995, *J. Geophys. Res.*, *105*, 14,677–14,700, 2000.

Marticorena, B., and G. Bergametti, Modeling the atmospheric dust cycle: 1. Design of a soil-derived dust emission scheme, *J. Geophys. Res.*, *100*, 16,415–16,430, 1995.

McTainsh, G. H., Dust storm index, in *Sustainable Agriculture: Assessing Australia's Recent Performance*, *SCARM Tech. Rep. 70*, 6752 p., Collingwood, Victoria, Australia, 1998.

McTainsh, G. H., J. F. Leys, and W. G. Nickling, Wind erodibility of arid lands in the Channel Country of western Queensland, Australia, *Z. Geomorphol. N.F.*, *116*, 113–130, 1999.

Penner, J. E., et al., Aerosols, their direct and indirect effects, in *Climate Change 2001: The Scientific Basis. Contribution of Working Group I to the Third Assessment Report of the Intergovernmental Panel on Climate Change*, edited by J. T. Houghton et al., chap. 5, pp. 291–336, Cambridge Univ. Press, New York, 2001.

Prospero, J. M., The atmospheric transport of particles to the ocean, in *Particle Flux in the Ocean*, edited by V. Ittekkot et al., SCOPE, 57, 19–52, 1996.

Prospero, J. M., P. Ginoux, O. Torres, S. E. Nicholson, and T. E. Gill, Environmental characterization of global sources of atmospheric soil dust derived from the NIMBUS 7 Total Ozone Mapping Spectrometer (TOMS) absorbing aerosol product, *Rev. Geophys.*, *40*(1), 1002, doi:10.1029/2000RG000095, 2002.

Rasch, P. J., W. D. Collins, and B. E. Eaton, Understanding the Indian Ocean Experiment INDOEX aerosol distributions with an aerosol assimilation, *J. Geophys. Res.*, *106*, 7337–7355, 2001.

Savoie, D. L., J. M. Prospero, S. J. Oltmans, W. C. Graustein, K. K. Turekian, J. T. Merrill, and H. Levy II, Sources of nitrate and ozone in the marine boundary layer of the tropical North Atlantic, *J. Geophys. Res.*, *97*, 11,575–11,589, 1992.

Schulz, M., Y. Balkanski, W. Guelle, F. Dulac, C. Moulin, and C. E. Lambert, Model components necessary to capture a dust plume pattern over the Mediterranean Sea, in *The Impact of Desert Dust Across the Mediterranean*, edited by S. Guerzoni and R. Chester, pp. 51–58, Kluwer Acad., Norwell, Mass., 1996.

Schulz, M., Y. J. Balkanski, W. Guelle, and F. Dulac, Role of aerosol size distribution and source location in a three-dimensional simulation of a Saharan dust episode tested against satellite-derived optical thickness, *J. Geophys. Res.*, *103*, 10,579–10,592, 1998.

Seinfeld, J. H., and S. N. Pandis, *Atmospheric Chemistry and Physics*, John Wiley, New York, 1997.

Tegen, I., P. Hollrig, M. Chin, I. Fung, D. Jacob, and J. Penner, Contribution of different aerosol species to the global aerosol extinction optical thickness: Estimates from model results, *J. Geophys. Res.*, *102*, 23,895–23,915, 1997.

Torres, O., P. K. Bhartia, J. R. Herman, Z. Ahmad, and J. Gleason, Derivation of aerosol properties from satellite measurements of backscattered ultraviolet radiation: Theoretical basis, *J. Geophys. Res.*, *103*, 17,099–17,110, 1998.

Torres, O., P. K. Bhartia, J. R. Herman, A. Sinyuk, P. Ginoux, and B. Holben, A long-term record of aerosol optical depth from TOMS observations and comparison to AERONET measurements, *J. Atmos. Sci.*, *59*, 398–413, 2002.

White, B. R., Soil transport by winds on Mars, *J. Geophys. Res.*, *84*, 4643–4651, 1979.

Woodward, S., Modeling the atmospheric lifecycle and radiative impact of mineral dust in the Hadley Centre climate model, *J. Geophys. Res.*, *106*, 18,155–18,166, 2001.

Zender, C. S., H. Bian, and D. Newman, Mineral Dust Entrainment and Deposition (DEAD) model: Description and 1990s dust climatology, *J. Geophys. Res.*, *108*(D14), 4416, doi:10.1029/2002JD002775, 2003.

D. Newman and C. S. Zender, Department of Earth System Science, University of California at Irvine, Irvine, CA 92697-3100, USA. (zender@uci.edu)

O. Torres, Joint Center for Earth Systems Technology, University of Maryland Baltimore County, Baltimore, MD 21250, USA.